ANALYSIS AND MITIGATION OF CALCIUM ARTIFACTS IN CARDIAC MULTIDETECTOR CT

*Zhuangli Liang, W. Clem Karl**

Boston University
Department of
Electrical and Computer Engineering
Boston, MA

Synho Do, Thomas Brady, Homer Pien

Massachusetts General Hospital
Department of Radiology
Boston, MA

ABSTRACT

Multi-detector Computed Tomography offers the promise of a non-invasive alternative to invasive coronary angiography for the evaluation of coronary artery disease. An impediment preventing its widespread adoption is the presence of image "blooming" artifacts due to the presence vascular calcium. This blooming has been linked to cardiac motion, beam hardening, and resolution effects. In this paper we study the contribution of these elements to blooming in a controlled way and conclude that the strongest effect for current systems is due to resolution. We then present a multi-component algebraic-type reconstruction approach to mitigate such blooming artifacts, motivated by recent results in image inpainting. The reconstruction approach decomposes the image into a collection of spatially localized components, each with a set of homogeneous properties. The local nature of the decomposition and constraints prevents artifacts from contaminating other image regions.

Index Terms— Cardiac CT, MDCT, calcium blooming

1. INTRODUCTION

Atherosclerosis of the coronary arteries is the major cause of morbidity and mortality in industrialized nations. Coronary angiography is the gold standard for evaluation of coronary stenosis, with 1.7 million diagnostic procedures being performed in 2001. Unfortunately, angiography is invasive and has a significant rate of complication. Multi-detector Computed Tomography (MDCT) has seen increasing interest as a non-invasive surrogate for assessing stenosis and characterizing plaque in coronary artery disease. Historically, motion related artifacts have been the major limitation in the use of MDCT for cardiac imaging, but recent advances in scanner design which have reduced scanning time, coupled with improved clinical protocols during acquisition have substantially reduced these problems. The pervasive existence of blooming artifacts, due to the presence of coronary calcium deposits, has emerged as a significant problem preventing the acceptance of MDCT as an alternative to invasive angiography. This blooming exaggerates the apparent size of vascular occlusions and confounds reliable identification of stenotic regions of the vascular tree, as shown in Fig. 1.

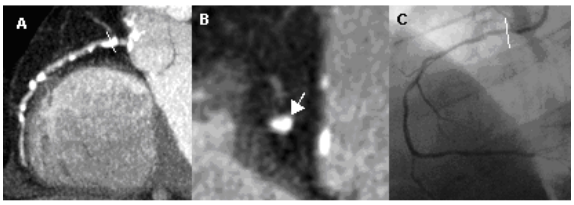

Fig. 1. False positive MDCT for significant stenosis. (a) Axial thin slice MIP (5mm) MDCT image shows large calcified plaque in the proximal RCA (line). (b) Cross sectional image of the RCA confirms large calcification, apparently without residual contrast filled lumen. (c) Invasive coronary angiography demonstrates no significant obstruction of the lumen.

Causes for the blooming include beam hardening, cardiac motion, and resolution effects. In this paper we study the contribution to blooming caused by these elements in a controlled way and conclude that the dominant cause is resolution, followed by motion, with beam hardening effects being negligible. We present a multi-component algebraic-type reconstruction approach to mitigate such blooming artifacts, motivated by recent results in image inpainting. The reconstruction approach decomposes the image into a collection of spatially localized components, each with a set of homogeneous properties. The local nature of the decomposition and constraints prevents artifacts from contaminating other image regions.

2. ANALYSIS OF CALCIUM BLOOMING EFFECTS

In this section we study calcium blooming artifacts in cardiac CT imagery. Three effects have been linked to calcium

*This work was supported in part by the Center for Integration of Medicine and Innovative Technology (CIMIT), and by the NSF funded Engineering Research Center for Subsurface Sensing and Imaging Systems. Siemens Medical provided the DRASIM simulation package and made details of the Sensation-64 MDCT available to us.

blooming in cardiac CT images: 1) beam hardening, 2) motion effects, and 3) resolution and partial volume effects. We used the CT simulation suite DRASIM (Siemens Medical, Forchheim) in a controlled simulation study of these effects. DRASIM is a simulator of X-ray transmission through complex geometric phantoms of arbitrary material. It is a fully 3-D simulation package which calculates X-ray beam attenuation based on narrow beam cross sections taken from the NEA/LLNL Evaluated Nuclear Data Libraries as found in the EADL (Evaluated Atomic Data Library) and EPDL (Evaluated Photon Data Library) [1].

For simplicity and speed in this study, we used a two-dimensional, single-slice geometry with nominal parameters chosen to mimic a state of the art, Siemens Sensation-64, double threaded spiral cone-beam CT scanner with 1160 projections per rotation, 672 channels per slice, collimated slice thickness at the isocenter of $0.6mm$, and a rotation time of 0.33s [2]. Since we focused on simulation of small objects near the isocenter, a parallel geometry was used. The associated detector size was adjusted to match the corresponding nominal detector cross-section of $0.77mm$ at the isocenter of the Sensation-64. The projection data was reconstructed using a parallel FBP program supplied by Siemens Medical Systems. This program is embedded with different body kernels used in the Sensation-64 scanner and allowed validated kernel effects to be included. The kernel used in this study was the standard B35f kernel used in cardiac imaging protocols.

To study blooming a numerical phantom was used to model a small half-circle of calcium centered in a background region of water. The calcium had a diameter of $2mm$ and density of 1400HU, while the background had a diameter of $20mm$ and a density of 0HU. To decouple reconstruction resolution effects from more fundamental detector size effects, we performed all our reconstructions on a very fine fixed grid size of $0.04mm$/voxel. We measured calcium blooming by calculating the subsequent area of the calcium in the reconstructed image and comparing it to the true area ($\pi/2$ mm^2). The calcium area was found as the area of the image above a fixed threshold of 250HU. In what follows images are displayed in a range of [-225,575]HU unless otherwise stated.

2.1. Beam Hardening

In this section we examine the effect of beam hardening on calcium blooming. While DRASIM can model the two cases of a polychromatic or monochromatic X-ray source, we wanted to examine a continuous range of beam hardening effects. To this end, we instead used a fixed polychromatic source spectrum and embedded the above calcium phantom inside a 40mm thick ring of material whose density we then varied (Fig. 2a). As the density of the material in the ring increases, a larger beam hardening effect on the calcium phantom is obtained as the energy reaching this region is hardened.

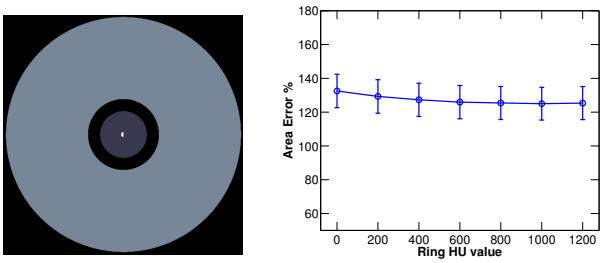

Fig. 2. Effect of beam hardening. From left to right, (a) True image with material ring. (b) Calcium area error as function of material density.

Fig. 2b shows how the calcium area error varies as the amount of beam hardening is changed from none (corresponding to ring density of 0HU) to maximum (corresponding to a ring density of 1200HU) at the nominal isocenter detector size of $0.77mm$. The effect is very weak, producing some actual reduction in area. This small reduction in area is due to the apparent reduction in estimated calcium density because of the beam hardening coupled with a fixed intensity threshold. Overall, the beam hardening effect is negligible. Note here that we have focused only on the area effect of beam hardening, and not other changes to visual appearance that may result in challenging image interpretation in practice.

2.2. Motion Effects

In this section we examine the effect of motion on calcium blooming. We used the empirical motion function from [3] and illustrated in Fig. 3a to define a 2-D linear motion. Although this motion is simplified, it captures the characteristics of different cardiac phases and velocities seen in the literature. Images were reconstructed at 65% of the R-R cycle, where the motion is slow, representing mid-diastole. Figs. 3b and 3c show reconstructed images at two different heart rates. Fig. 3d shows how calcium area error varies as a function of heart rate for different detector sizes. It can be seen that the impact of motion on area error is related to detector size, with motion becoming more important as resolution increases. At high resolutions (small detector size), motion effects can be significant, but at nominal resolutions (detector size of $0.77mm$) and nominal heart rates (65 BPM) the additional area error introduced by motion is minimal. While motion can also introduce more complicated morphological changes to structures, we have focused here only on the area effect of motion.

2.3. Resolution Effects

We now examine the effect of scanner resolution on reconstructed calcium area error. We computed the calcium area error from images reconstructed using a range of detector resolutions from the nominal detector resolution ($0.77mm$) to 1/4 the nominal detector resolution ($0.19mm$). The dose was

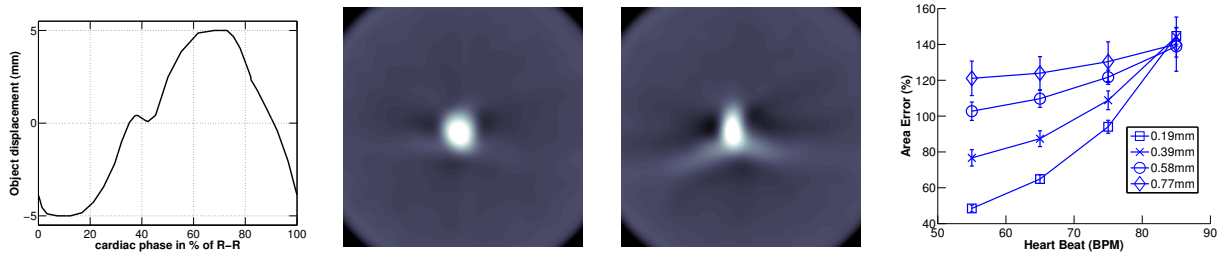

Fig. 3. Effect of motion. From left to right, top to bottom, (a) The 2D linear motion function used. (b) Image for 65% R-R, 55 BPM (c) Image for 65% R-R, 85 BPM (d) Calcium area error vs. heart rate for different detector sizes

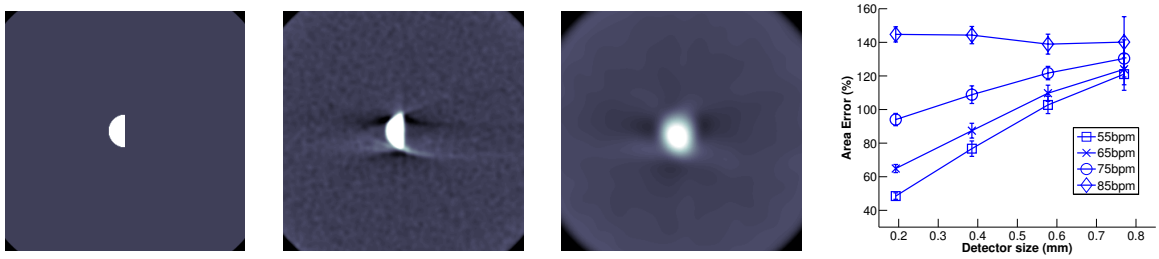

Fig. 4. Effect of detector size. From left to right, top to bottom, (a) True image (b) Image with detector size 1/4 of nominal (0.19mm) (c) Image with nominal detector size (0.77mm) (d) Calcium area error vs. detector size for different heart rates

adjusted so that the product of source mAs and detector size was kept constant. Fig. 4a shows the underlying true phantom. Figs. 4b and 4c show images at two detector resolutions. Even though the reconstructions include the smoothing introduced by the B35f kernel, the higher detector resolution exhibits very little blooming effect. Fig. 4d shows how the reconstructed calcium area error varies as a function of detector resolution for different heart rates. When the heart rate is very high, motion effects dominate, showing the importance of controlling heart rate. At nominal heart rates (65 BPM), and near nominal resolutions, incremental changes in resolution appear to have a larger effect.

2.4. Relative Effect Evaluation

From the above discussion, the two dominant contributions to blooming appear to be motion and resolution, with beam hardening having only a small effect. To further understand the relative contribution of motion and resolution, let us define a nominal heart rate of 65BPM and a nominal resolution of $0.77mm$. These values represent typical "operating points" of current MDCT cardiac systems (i.e. protocol controlled heart rate and native scanner resolution). Similarly, let us define an ideal heart rate of 55BPM and an ideal resolution of $0.19mm$ (1/4 nominal). These values are meant to represent limiting, ideal values of these parameters. From our graphs we can extract the area errors corresponding to various combinations of these nominal and ideal parameters, which we summarize in Table 1. From the table we can see that nominal MDCT conditions produce an area error of approximately 125%. Reducing the motion from its nominal value to its ideal value only reduces this error by 5%, while improving resolution from its nominal to ideal value reduces the error by nearly a factor of two. Overall, resolution improvements appear to have a larger effect than motion improvements by a significant amount.

Area Errors		Resolution	
		Nominal	Ideal
Motion	Nominal	125%	65%
	Ideal	120%	50%

Table 1. Sensitivity of area errors to blooming effects

3. MITAGATION OF BLOOMING

In this section use an algebraic-type reconstruction approach to mitigate calcium blooming by focusing or containing the intensity associated with the hyper-dense calcium. We decompose the underlying scene into a collection of components, each of which has a homogeneous property. Such a decomposition has been successfully used for image inpainting [4], and we apply this idea to tomographic artifact mitigation. Prior information on the behavior of each component texture can be included in the reconstruction process and the behavior of one region is prevented from contaminating adjacent regions. We couple this underlying multi-component scene model with a tomographic sensing model to perform joint image formation and artifact suppression through an iterative re-

construction approach. Detailed development of the method is the focus of a subsequent paper. Iterative approaches to CT have shown great promise in dealing with a variety of challenges, including polyenergetic sources [5], metal artifacts [6], and missing data [7].

3.1. Reconstruction Approach

For simplicity we focus on a two-component model. We decompose the overall underlying scene as the sum of these components: $f = f_c + f_s$, where f_c corresponds to the hyperdense calcium component and f_s corresponds to the remaining background component. We reconstruct an image by minimizing an energy function composed of three terms:

$$\widehat{f} = \arg\min_f E_d(g, f) + \alpha_s E_s(f_s) + \alpha_c E_c(f_c) \qquad (1)$$

The first term $E_d(g, f)$ captures fidelity to the observed projection data, and incorporates our model of the projection process. In particular, we choose it to be the log-likelihood of the projection data. The second term $E_s(f_s)$ captures our prior knowledge of the behavior of the background, non-calcified tissue component. This component is believed to be relatively smooth, so we make a common choice of $E_s(f_s) = \|Df_s\|^2$, where D is a discrete approximate to a derivative operator. The last term $E_c(f_c)$ captures our prior knowledge of the behavior of calcium deposits. We assume the calcium component is sparsely distributed and highly concentrated. In preliminary work we have chosen $E_c(f_c) = \|Df_c\|_1^1$ to focus the calcium component [8]. In Fig. 5 we show a preliminary result of the approach on an in vivo image of a subject with two coronary stents. The left image shows the conventional scanner generated image while the right image shows the result of our new approach. Below these are enlargements of one of the stents. In the conventional imagery the dense metallic stent has bloomed and the lumen does not appear open. In our result the lumen appears open.

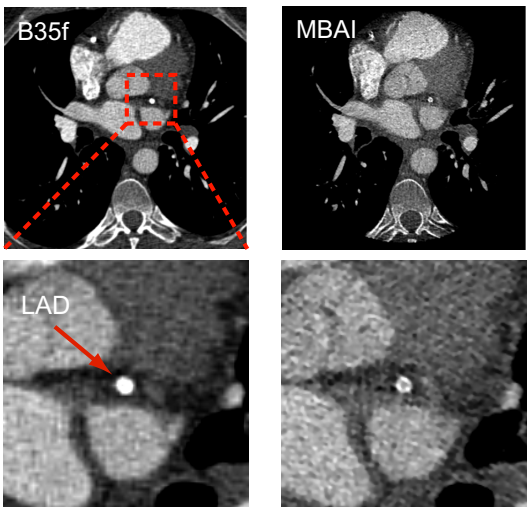

Fig. 5. In Vivo Example comparing stent region in conventional and MBAI reconstructions.

4. CONCLUSIONS

In this paper we studied the contribution to calcium blooming of cardiac motion, beam hardening, and resolution effects. While all these effects create artifacts, the dominant cause of such calcium blooming appears to be due to limited detector resolution. We then used a multi-component algebraic-type reconstruction approach to mitigate such calcium derived artifacts. The method defines the reconstructed image as series of components with different properties. We exploit this decomposition to minimize the blooming effect while retaining the characteristics of the background.

5. REFERENCES

[1] S. T. Perkins and D. E. Cullen, "Endl type formats for the llnl evaluated atomic data library, eadl for the evaluated electron data library, eedl, and the evaluated photon data library," Tech. Rep. EPDL UCRL-ID-117796, University of California, July 1994.

[2] M. Kachelriess, M. Knaup, P. Pensel, and W. A. Kalender, "Flying focal spot (ffs) in cone-beam ct," *IEEE Trans. Nuclear Science*, vol. 53, pp. 1238–1247, June 2006.

[3] T. G. Flohr, C. H. McCollough, H. Bruder, M. Petersilka, K. Gruber, C. Suss, M. Grasruck, K. Stierstorfer, B. Krauss, R. Raupach, A. N. Primak, A. Kuttner, S. Achenbach, C. Becker, A. Kopp, and B. M. Ohnesorge, "First performance evaluation of a dual-source ct (dsct) system," *European Radiology*, vol. 16, pp. 256–268, 2006.

[4] M. Bertalmio, L. Vese, G. Sapiro, and S. Osher, "Simultaneous structure and texture image inpainting," *IEEE Transactions on Image PRocessing*, vol. 12, pp. 882–889, 2003.

[5] I. A. Elbakri and J. A. Fessler, "Statistical image reconstruction for polyenergetic x-ray computed tomography," *IEEE Trans. Medical Imaging*, vol. 21, no. 2, pp. 89–99, Feb. 2002.

[6] G. Wang, D. L. Snyder, J. A. O'Sullivan, and M. W. Vannier, "Iterative deblurring for ct metal artifact reduction," *IEEE Trans. Medical Imaging*, vol. 15, no. 5, pp. 657–664, Oct. 1996.

[7] P.E. Kinahan, J. A. Fessler, and J. S. Karp, "Statistical image reconstruction in pet with compensation for missing data," *IEEE Trans. Nuclear Science*, vol. 44, no. 4, pp. 1552–1557, Aug. 2997.

[8] D. Donoho, "Superresolution via sparsity constraints," *SIAM Journal of Mathematical Analysis*, vol. 23, pp. 1309–1331, 1993.